Preparation of Long-Lived, Non-Autoionizing Circular Rydberg States of Strontium

R. C. Teixeira,[1,2] A. Larrouy,[1] A. Muni,[1] L. Lachaud,[1] J.-M. Raimond,[1] S. Gleyzes,[1,*] and M. Brune[1]
[1]Laboratoire Kastler Brossel, Collège de France, CNRS, ENS-Université PSL, Sorbonne Université, 11, place Marcelin Berthelot, 75005 Paris, France
[2]Departamento de Física, Universidade Federal de São Carlos, Rodovia Washington Luís, km 235—SP-310, 13565-905 São Carlos, São Paulo, Brazil

(Received 30 June 2020; accepted 1 December 2020; published 28 December 2020)

Alkaline earth Rydberg atoms are very promising tools for quantum technologies. Their highly excited outer electron provides them with the remarkable properties of Rydberg atoms and, notably, with a huge coupling to external fields or to other Rydberg atoms while the ionic core retains an optically active electron. However, low angular-momentum Rydberg states suffer almost immediate autoionization when the core is excited. Here, we demonstrate that strontium circular Rydberg atoms with a core excited in a $4D$ metastable level are impervious to autoionization over more than a few millisecond time scale. This makes it possible to trap and laser-cool Rydberg atoms. Moreover, we observe singlet to triplet transitions due to the core optical manipulations, opening the way to a microwave to optical quantum interface.

DOI: 10.1103/PhysRevLett.125.263001

Rydberg atoms are a promising platform for quantum information [1], quantum metrology [2,3], or quantum simulation [4,5]. Most Rydberg atom experiments have been using alkali metals. However, alkaline-earth Rydberg atoms are now the focus of an intense experimental activity [6]. In the context of alkaline-earth-based optical atomic clocks, dressing with or excitation to Rydberg states open promising perspectives for noise reduction by the preparation of atomic ensemble nonclassical states [7,8]. Rydberg states spectroscopy leads to estimations of the systematic shift of these clocks induced by the blackbody radiation or by residual electric fields [9–11]. More importantly, in the alkaline-earth Rydberg states, the optically active ionic core makes it possible to image [12,13] or trap [14,15] atoms, opening interesting perspectives for quantum simulation [16,17].

Most alkaline-earth experiments, so far, access low-angular-momentum Rydberg states [18–20], for which the core excitation quickly leads to autoionization [21,22]. Overcoming this limit requires increasing the angular momentum ℓ of the Rydberg electron [13]. Moderately large-ℓ states have been produced using microwave (mw) transfer [23] or Stark switching methods. Early studies [24–27] have evidenced the reduction of the autoionization rate with ℓ but extending them to $\ell > 10$ is challenging [28].

The circular states of alkaline-earth atoms are expected to offer the best protection against autoionization. Circular Rydberg levels [29,30] have the maximum allowed magnetic quantum number, $m = \ell = n - 1$. They have remarkable properties, in particular, a long intrinsic lifetime (30 ms for $n = 50$). They were used extensively to manipulate microwave fields in superconducting cavities [31]. They have recently attracted a broader interest, from cold atom physics [32] to quantum metrology [3,33] or quantum simulation [34]. Finally, their wave function is localized at a large distance from the core. Hence, the outer electron of an alkaline-earth circular state has a minute overlap with the core. The autoionization rate is expected to be extremely low. An early study of the $n = 21$ circular state of Barium had already exhibited reduced autoionization for a core in one of its metastable levels [35]. Their low autoionization rate, combined with their unique properties, explains the interest for alkaline-earth circular states in recent proposals [15,36].

In this Letter, we report an important experimental step in the control of alkaline-earth Rydberg atoms, with the preparation of the $n = 51$ singlet circular state of strontium. We observe transitions to the triplet states resulting from a selective manipulation of the ionic core electron. We observe negligible autoionization when the core electron is promoted to any of the $4D$ metastable states. These results open bright perspectives for optical manipulation of circular Rydberg states.

The strontium circular Rydberg states are produced from a thermal atomic beam inside an electrode structure controlling the static electric field at the atomic position [Fig. 1(a)]. The experiment is cooled down to 4.2 K by a wet ^{4}He cryostat. The atoms are promoted from the $5s^2\,{}^1S_0$ singlet ground state to the $5s52f\,{}^1F_3$, $m = 2$ Rydberg state by a stepwise resonant three-photon excitation (461, 767, and 896 nm) using $5s5p\,{}^1P_1$ and $5s5d\,{}^1D_2$ as intermediate states [37]. The lasers selectively excite the ^{88}Sr isotope [38]. After excitation in the Rydberg states, a 422 nm laser pulse can excite the second, core valence electron at a wavelength close to the $5S_{1/2} \rightarrow 5P_{1/2}$ resonance of Sr^+.

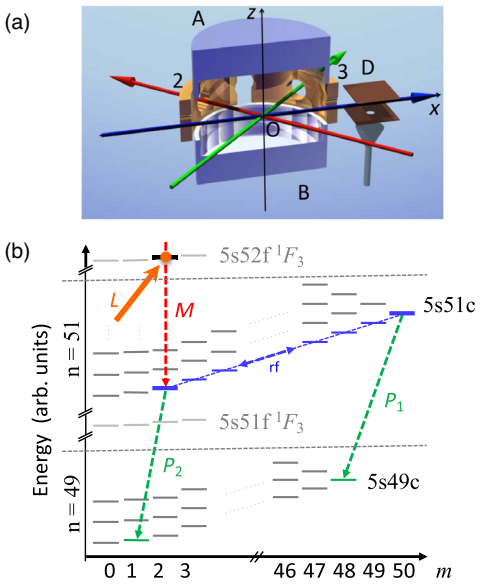

FIG. 1. (a) Experimental setup. The thermal atomic beam (blue arrow) intersects the laser beams (767 and 896 nm in green and 461 and 422 nm in red) in the center of the electrode structure. Two electrodes A and B create the vertical electric field, four electrodes 1, 2, 3, and 4 (1 and 4 not shown) generate the σ^+-polarized rf field. The atoms are detected in the ionization detector D. (b) Relevant levels of the Rydberg manifolds. The laser pulse L prepares the $5s52f^1F_3$, $m = 2$ sublevel (orange dot). The dashed lines M, P_1, and P_2 represent microwave pulses, the blue dashed lines the rf transitions.

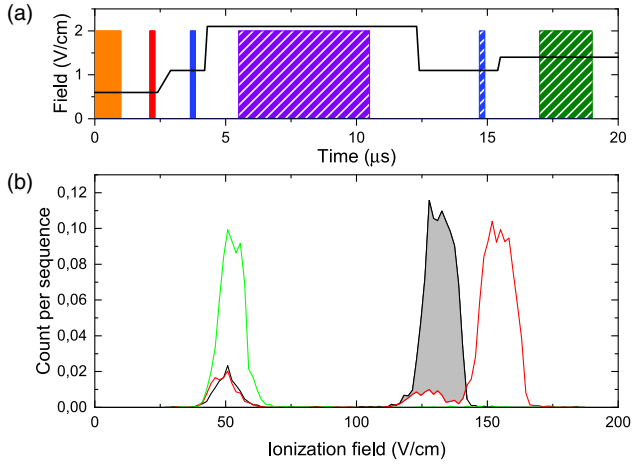

FIG. 2. (a) Experimental timing. Orange, red, blue, violet, and green areas correspond to laser excitation, mw preparation, rf pulse, 422 nm laser and mw probe pulses, respectively. Events with hatched areas are not applied for the data presented in Fig. 2(b). (b) Ionization signals. Number of detected atoms as a function of the ionization voltage after the microwave preparation pulse M pulse (green), after the circularization rf pulse (black), after the rf pulse and the probe mw pulse P_1 (red). The difference between the black and red curves (shaded area) corresponds to the atoms in the $5s51c$.

For alkali atoms [30], the transfer from the laser-accessible state to the circular state involves a series of degenerate radio-frequency (rf) transitions between Stark levels. Because of its large quantum defect, the laser-excited $5s52f^1F_3$ strontium level is far from the hydrogenic manifold for fields on the order of $F \sim 1$ V/cm [Fig. 1(b)]. Thus, we transfer the atom from this level into the lowest $m = 2$ state of the $n = 51$ Stark manifold with a microwave π pulse (M). Then, we apply a σ^+-polarized rf "circularization" pulse, resonant with the transitions between the lowest levels in the Stark ladder [blue states in Fig. 1(b)]. It transfers the $m = 2$ level into the circular state. In the circular state, spin-orbit coupling and exchange interaction have a negligible effect over the experimental timescale. For all practical purposes, singlet and triplet states are degenerate. Since the process starts from a laser-excited singlet state and since the mw and rf fields conserve the electron spin, the atoms are prepared in the singlet state $5s51c$, $S = 0$.

Figure 2(a) shows a generic experimental timing. Figure 2(b) shows the ionization signals measured with the state-selective field-ionization detector at different steps in the preparation. Low-m levels prepared by the microwave pulse M ionize in a field $\simeq$50 V/cm (green line). After the circularization rf pulse, the atoms ionize in a much larger field, close to the expected circular-state ionization threshold (black line). The residual ionization peak at low field is mainly due to atoms left in the $5s52f^1F_3$ state by the imperfect mw pulse. Most of the population in the $n = 51$ manifold has, thus, been transferred to high-angular momentum states. Because of the Stark level anharmonicity for low m, the resonant rf pulse cannot prepare the circular state with unit efficiency [30]. In order to count the number of atoms in the circular state, we apply a mw probe pulse P_1 (red line) resonant with the two-photon $5s51c \rightarrow 5s49c$ transition between circular states but out-of-resonance for noncircular states [see Fig. 1(b)]. We measure that at least 85% of the atoms that ionize at high field are in the circular state [37].

Then, we check that the circular states are insensitive to autoionization when exciting the core. As the Rydberg electron is far away from the core, the core level structure should be nearly that of the Sr^+ ion [22]. The doubly excited states have the form $j_1, l_1, 51c$, where j_1, l_1 refer to the total and orbital angular momenta of the core electron. After the circularization rf pulse, we excite the core with the 422 nm laser beam tuned close to the $5S_{1/2} \rightarrow 5P_{1/2}$ transition of Sr^+. The beam has a Gaussian waist of 430 μm and a power P (maximum 16 mW). The interaction time is limited by the atomic transit across the beam. When the laser is on resonance, the atoms excited to $5p_{1/2}, 51c$ can decay into the $4d_{3/2}, 51c$ metastable state (branching ratio 1:17). Its lifetime is expected to be close to that of the $4D_{3/2}$ level of Sr^+ (0.4 s) [13]. For a large enough P, atoms should be optically pumped in this state and remain in it during their 140 μs flight toward the detector.

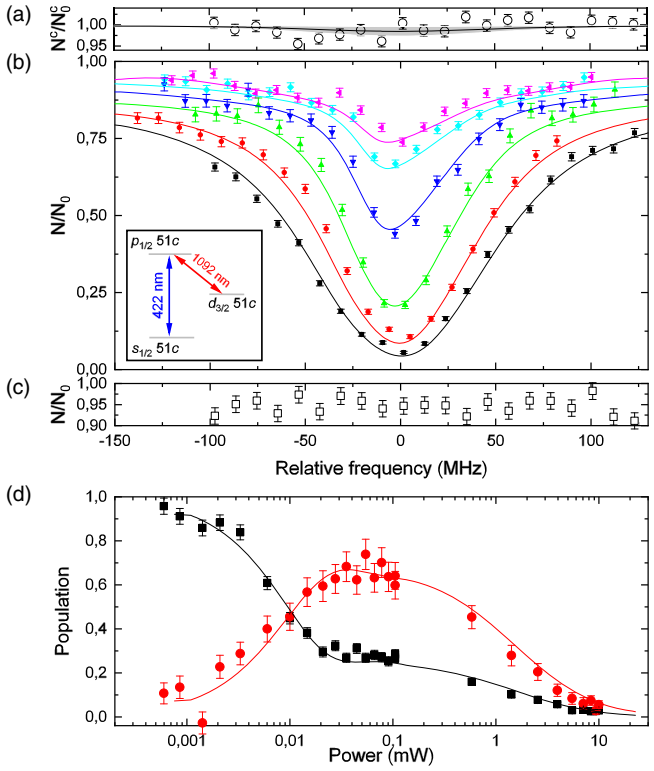

FIG. 3. (a) Normalized number N^c/N_0^c of atoms detected in the circular state $51c$ after applying the 422 nm laser pulse as a function of its relative frequency $\Delta\nu_l$. The laser power is $P = 16$ mW. The normalization factor N_0^c is the number of $51c$ atoms measured without this laser pulse. The frequency reference is arbitrary. The points are experimental with statistical error bars. The shadowed area corresponds to the 95% confidence band of the fit of the survival probability (solid line, see text). (b) Normalized number N/N_0 of atoms detected in low-m states after decircularization rf pulse as function of $\Delta\nu_l$ for different laser powers (black: 16 mW, red: 9.5 mW, green: 4.0 mW, blue: 1.3 mW, cyan: 0.5 mW, magenta: 0.3 mW). The slight asymmetry at low power is due to the asymmetry of the atomic velocity distribution [37]. The inset shows the relevant levels. (c) Normalized number N/N_0 for $P = 16$ mW with 1092 nm repumper light. (d) Population of the $5s_{1/2}$, $51c$ singlet (p_S, black) and triplet (p_T, red) states as a function of the 422 nm laser power P when it is set at resonance. (b)–(d) The points are experimental (with statistical error bars) and the lines are the predictions of the numerical model.

Figure 3(a) presents the population left in the circular state as a function of the relative frequency $\Delta\nu_l$ of the 422 mn laser. It is nearly constant within measurement uncertainties. Thus, autoionization is negligible over a 140 μs timescale.

Now, we indirectly probe the fraction of atoms optically pumped in $4d_{3/2}$, $51c$ by applying a "decircularization" rf pulse [hatched blue pulse on Fig. 2(a)]. It transfers the $5s_{1/2}$, $51c$ singlet circular state back to low-m states. We count the number of $n = 51$ Rydberg atoms detected at the $m = 2$ ionization threshold. When the core is excited, atoms with $m \approx 2$ autoionize immediately. Thus, we count only the atoms left in $5s_{1/2}$ after the 422 nm laser pulse.

Figure 3(b) presents the number of detected atoms, N, normalized by the number N_0 of atoms detected without applying the 422 nm laser [37]. As expected, we observe a resonance dip, whose depth increases with the blue laser power, P. As an additional check, we perform the same experiment with an additional 1092-nm "repumper" light, saturating the $4d_{3/2}$, $51c \rightarrow 5p_{1/2}$, $51c$ transition [level diagram in the inset of Fig. 3(b)]. Its polarization is modulated at 3 MHz in order to empty all m_j sublevels of $4d_{3/2}$, $51c$ [39]. We observe a flat signal, close to 100% [Fig. 3(c)], confirming that the dip in Fig. 3(b) is due to optical pumping in $4d_{3/2}$, $51c$.

The data are in excellent agreement with numerical simulations computing the population of $5s_{1/2}$, $51c$ before the decircularization rf pulse [solid lines in Fig. 3(b)]. They are based on a model of optical pumping by the 422 nm laser within the magnetic sublevels of the s and p core states. We take into account the velocity distribution and the spatial extension of the atomic sample. The only adjustable parameter is a proportionality factor between the 422 nm laser power P and its intensity at the atomic position. We fit it to be 26% smaller than the expected value. The discrepancy is likely due to the uncertainty on the exact geometry of the excitation lasers inside the cryostat [37].

For the $5p_{1/2}$, $51c$ state, the spin-orbit coupling of the core electron is dominant with respect to the exchange interaction. Scattering photons at 422 nm may flip the core electron spin. The atom decaying back into $5s_{1/2}$, $51c$ ends up in a statistical mixture of singlet and triplet states. As the exchange energy is not negligible for low-m states, the efficiency of the decircularization rf pulse is different for atoms in the $5s_{1/2}$, $51c$ singlet or triplet states. Thus, the model uses a detection efficiency of the $5s_{1/2}$, $51c$ triplet state equal to 93% of that of the singlet. Note that the efficiency of the decircularization rf pulse might change when the core is in $4d_{3/2}$. However, $4d_{3/2}$ atoms left in states with $m > 2$ either autoionize or have an ionization threshold too large to be detected. Thus, the $4d_{3/2}$ atoms do not contribute to the signal.

The exchange energy for low-m states makes it possible to use the Rydberg electron to probe the core electron spin dynamics. After the decircularization pulse, we apply a selective mw probe pulse [green rectangle in Fig. 2(a)] transferring either the singlet or triplet $n = 51$, $m = 2$ lowest state into the $n = 49$ manifold. The number of atoms detected in $n = 49$ after the probe pulse allows us to reconstruct the populations p_S and p_T of the singlet and triplet $5s_{1/2}$, $51c$ states at the end of the optical pumping process [37]. Figure 3(d) presents the evolution of these populations with P when the 422 nm laser is on resonance and the 1092 nm repumper is not applied. The solid lines

present the predictions of the model. They are in excellent agreement with the data.

We observe two regimes. Up to $P = 0.1$ mW, the singlet state population decreases with P down to ~25%, while the triplet state population rises to ~75%. Indeed, the 422 nm laser polarization has been chosen to be nearly σ^- (for the core state, we consider a quantization axis along the 422 nm laser direction). Thus, the $5s_{1/2}$, $m_j = -1/2$ sublevel is almost a dark state [39], into which the core electron is optically pumped after a few absorption-spontaneous emission cycles only. The final state of the optical pumping process is, thus, a 1:3 mixture of singlet and triplet states.

For higher powers, $P > 0.1$ mW, the small σ^+ component of the 422 laser polarization (the ratio between the σ^+ and σ^- intensities is measured to be 1:36) becomes large enough to have a sizable effect. The $5s_{1/2}, m_j = -1/2$ state is no longer a dark state. Absorption and spontaneous emission cycles go on until the atoms fall in the $4d_{3/2}, 51c$ metastable state. Accordingly, both singlet and triplet populations decrease with P. For the largest power, we estimate that 95% of the atoms are in the metastable core state before the decircularization pulse is applied.

The optical pumping model combined with the data of Fig. 3(a) allows us to estimate a lower bound for the autoionization lifetime of $4d_{3/2}$, $51c$. On the signal of Fig. 3(a), we fit a dip proportional to the number of atoms in $4d_{3/2}$, $51c$ provided by the model. The dip depth is between 0.4% and 2.7% (95% confidence level). For a 140 μs time of flight, this corresponds to an autoionization lifetime larger than 5 ms [37].

We briefly investigate the $4d_{5/2}$, $51c$ autoionization lifetime. We repeat the experiment corresponding to that of Figs. 3(a) and 3(b) with a cw 408 nm laser exciting the atom into the $5p_{3/2}$, $51c$ level, instead of the 422 nm laser. The 408 nm laser is a free-running frequency-doubled Ti:Sa laser [37], with a power P' on the order of a milliwatt, sufficient to optically pump the atoms into $4d_{5/2}$, $51c$ since the $5s_{1/2} - 5p_{3/2}$ transition does not have a dark state for any polarization [39].

Figure 4 presents the circular state survival probability, as well as the number of atoms detected in low-m states after the decircularization rf pulse, as a function of the 408 nm laser frequency. To eliminate the effect of the slow drift of this frequency [37], the two curves are recorded simultaneously. As for Fig. 3, we observe no significant variation on Fig. 4(a) and a deep dip in Fig. 4(b) due to autoionization when we return to low-m states after core excitation. Note that the $5p_{3/2}$, $51c$ state decays into both $4d_{5/2}$, $51c$ and $4d_{3/2}$, $51c$ levels with rates r and r', respectively [inset of Fig. 4(b)]. The branching ratio $r/r' = 8.4$ measured in Sr^+ [40] indicates that the atoms are mostly pumped into $4d_{5/2}$, $51c$ [37].

We get an estimate of the $4d_{5/2}$, $51c$ autoionization lifetime by fitting the data of Fig. 4(b) with a Lorentzian

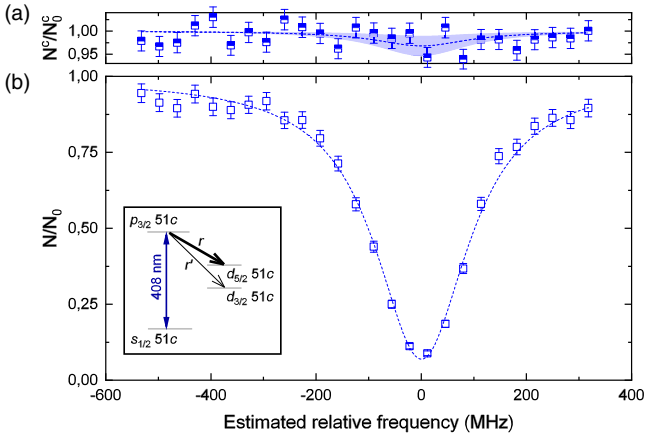

FIG. 4. Survival probability N^c/N_0^c (a) and N/N_0 (b) in the presence of 408 nm light as a function of the laser frequency. The points are experimental with statistical error bars. The dashed lines are Lorentzian fits of both curves with the same width and center frequency. The baselines of the fits are set to 1. The shadow area in (a) corresponds to the 95% confidence band of the fit. The inset shows the relevant ionic core levels.

line shape (dashed line). The dip depth corresponds to the fraction of the atoms optically pumped in the metastable states (within a factor close to 1, due to different detection efficiencies of the singlet and triplet states). In order to estimate the survival probability of $4d_{5/2}$, $51c$, we fit the data of Fig. 4(a) with a Lorentzian line shape with the same center frequency and width as in (b). The fit confidence band gives a 2 ms lower bound for the autoionization lifetime [37].

We have prepared the circular state of strontium with $n = 51$ and observed extremely long autoionization lifetimes when the core electron is excited to any of the metastable $4d$ states. This is in contrast to the microsecond lifetime of the $5d_{5/2}$, $21c$ Barium state [35]. The measured lower bounds on the lifetimes (5 and 2 ms for the $4d_{3/2}$, $51c$ and $4d_{5/2}$, $51c$ states, respectively) are limited by the statistical uncertainty on the survival probability. The measurement precision could be considerably improved with cold atoms.

These results open the way to optical cooling and trapping of long-lived circular state atoms with considerable impact on quantum metrology and quantum simulation. The interaction between the core and Rydberg electron leads us to envision quantum logic operations between them. With optical manipulation techniques developed for ion trap experiments [41], these gate operations can be used to detect or manipulate the outer Rydberg electron, leading to a promising interface between optical and mw qubits.

We thank M. Poirier, Ch. Koch, and S. Patsch for fruitful discussions, I. Dotsenko, C. Sayrin, P. Méhaignerie for experimental support. Financial support from the Agence

Nationale de la Recherche under the Project No. "SNOCAR" (167754) is gratefully acknowledged. This publication has received funding from the European Union's Horizon 2020 under Grant Agreements No. 786919 (Trenscrybe) and No. 765267 (QuSCo).

*Corresponding author.
gleyzes@lkb.ens.fr

[1] M. Saffman, T. G. Walker, and K. Mølmer, Quantum information with Rydberg atoms, Rev. Mod. Phys. **82**, 2313 (2010).
[2] H. Fan, S. Kumar, J. Sedlacek, H. Kübler, S. Karimkashi, and J. P. Shaffer, Atom based RF electric field sensing, J. Phys. B **48**, 202001 (2015).
[3] A. Facon, E.-K. Dietsche, D. Grosso, S. Haroche, J.-M. Raimond, M. Brune, and S. Gleyzes, A sensitive electrometer based on a Rydberg atom in a Schrödinger-cat state, Nature (London) **535**, 262 (2016).
[4] H. Labuhn, D. Barredo, S. Ravets, S. de Léséleuc, T. Macrì, T. Lahaye, and A. Browaeys, Tunable two-dimensional arrays of single Rydberg atoms for realizing quantum Ising models, Nature (London) **534**, 667 (2016).
[5] H. Bernien, S. Schwartz, A. Keesling, H. Levine, A. Omran, H. Pichler, S. Choi, A. S. Zibrov, M. Endres, M. Greiner, V. Vuleti, and M. D. Lukin, Probing many-body dynamics on a 51-atom quantum simulator, Nature (London) **551**, 579 (2017).
[6] F. B. Dunning, T. C. Killian, S. Yoshida, and J. Burgdörfer, Recent advances in Rydberg physics using alkaline-earth atoms, J. Phys. B **49**, 112003 (2016).
[7] L. I. R. Gil, R. Mukherjee, E. M. Bridge, M. P. A. Jones, and T. Pohl, Spin Squeezing in a Rydberg Lattice Clock, Phys. Rev. Lett. **112**, 103601 (2014).
[8] R. Mukherjee, J. Millen, R. Nath, M. P. A. Jones, and T. Pohl, Many-body physics with alkaline-earth Rydberg lattices, J. Phys. B **44**, 184010 (2011).
[9] V. D. Ovsiannikov, A. Derevianko, and K. Gibble, Rydberg Spectroscopy in an Optical Lattice: Blackbody Thermometry for Atomic Clocks, Phys. Rev. Lett. **107**, 093003 (2011).
[10] W. Bowden, R. Hobson, P. Huillery, P. Gill, M. P. A. Jones, and I. R. Hill, Rydberg electrometry for optical lattice clocks, Phys. Rev. A **96**, 023419 (2017).
[11] T. Cantat-Moltrecht, R. Cortiñas, B. Ravon, P. Méhaignerie, S. Haroche, J.-M. Raimond, M. Favier, M. Brune, and C. Sayrin, Long-lived circular Rydberg states of laser-cooled Rubidium atoms in a cryostat, Phys. Rev. Research **2**, 022032 (2020).
[12] G. Lochead, D. Boddy, D. P. Sadler, C. S. Adams, and M. P. A. Jones, Number-resolved imaging of excited-state atoms using a scanning autoionization microscope, Phys. Rev. A **87**, 053409 (2013).
[13] P. McQuillen, X. Zhang, T. Strickler, F. B. Dunning, and T. C. Killian, Imaging the evolution of an ultracold strontium Rydberg gas, Phys. Rev. A **87**, 013407 (2013).
[14] A. D. Bounds, N. C. Jackson, R. K. Hanley, R. Faoro, E. M. Bridge, P. Huillery, and M. P. A. Jones, Rydberg-Dressed Magneto-Optical Trap, Phys. Rev. Lett. **120**, 183401 (2018).
[15] J. Wilson, S. Saskin, Y. Meng, S. Ma, A. Burgers, and J. Thompson, Trapped arrays of alkaline earth Rydberg atoms in optical tweezers, arXiv:1912.08754.
[16] A. Cooper, J. P. Covey, I. S. Madjarov, S. G. Porsev, M. S. Safronova, and M. Endres, Alkaline-Earth Atoms in Optical Tweezers, Phys. Rev. X **8**, 041055 (2018).
[17] M. A. Norcia, A. W. Young, and A. M. Kaufman, Microscopic Control and Detection of Ultracold Strontium in Optical-Tweezer Arrays, Phys. Rev. X **8**, 041054 (2018).
[18] J. Millen, G. Lochead, G. R. Corbett, R. M. Potvliege, and M. P. A. Jones, Spectroscopy of a cold strontium Rydberg gas, J. Phys. B **44**, 184001 (2011).
[19] S. Ye, X. Zhang, T. C. Killian, F. B. Dunning, M. Hiller, S. Yoshida, S. Nagele, and J. Burgdörfer, Production of very-high-n strontium Rydberg atoms, Phys. Rev. A **88**, 043430 (2013).
[20] S. Ye, X. Zhang, F. B. Dunning, S. Yoshida, M. Hiller, and J. Burgdörfer, Efficient three-photon excitation of quasi-one-dimensional strontium Rydberg atoms with n 300, Phys. Rev. A **90**, 013401 (2014).
[21] J. Millen, G. Lochead, and M. P. A. Jones, Two-Electron Excitation of an Interacting Cold Rydberg Gas, Phys. Rev. Lett. **105**, 213004 (2010).
[22] G. Fields, X. Zhang, F. B. Dunning, S. Yoshida, and J. Burgdörfer, Autoionization of very-high-n strontium Rydberg states, Phys. Rev. A **97**, 013429 (2018).
[23] F. Niyaz, J. Nunkaew, and T. F. Gallagher, Microwave spectroscopy of the Yb $6s(n+3)d \rightarrow 6sng, 6snh$, and $6sni$ transitions, Phys. Rev. A **99**, 042507 (2019).
[24] W. E. Cooke, T. F. Gallagher, S. A. Edelstein, and R. M. Hill, Doubly Excited Autoionizing Rydberg States of Sr, Phys. Rev. Lett. **40**, 178 (1978).
[25] R. R. Jones and T. F. Gallagher, Autoionization of high-l Ba $6p_{1/2}nl$ states, Phys. Rev. A **38**, 2846 (1988).
[26] L. Pruvost, P. Camus, J. M. Lecomte, C. R. Mahon, and P. Pillet, High angular momentum $6pnl$ and $6dnl$ doubly excited Rydberg states of barium, J. Phys. B **24**, 4723 (1991).
[27] D. Wehrli, M. Génévriez, and F. Merkt, Autoionization rates of core-excited magnesium Rydberg atoms in electric fields using the core fluorescence as a reference, Phys. Rev. A **100**, 012515 (2019).
[28] H. Lehec, X. Hua, P. Pillet, and P. Cheinet, Isolated core excitation of high orbital quantum number Rydberg states of ytterbium, arXiv:2005.09552 [Phys. Rev. A (to be published)].
[29] R. G. Hulet and D. Kleppner, Rydberg Atoms in "Circular" States, Phys. Rev. Lett. **51**, 1430 (1983).
[30] A. Signoles, E. Dietsche, A. Facon, D. Grosso, S. Haroche, J. Raimond, M. Brune, and S. Gleyzes, Coherent Transfer between Low-Angular-Momentum and Circular Rydberg States, Phys. Rev. Lett. **118**, 253603 (2017).
[31] J. M. Raimond, M. Brune, and S. Haroche, Manipulating quantum entanglement with atoms and photons in a cavity, Rev. Mod. Phys. **73**, 565 (2001).
[32] K. S. Kleinbach, F. Engel, T. Dieterle, R. Löw, T. Pfau, and F. Meinert, Ionic Impurity in a Bose-Einstein Condensate at Submicrokelvin Temperatures, Phys. Rev. Lett. **120**, 193401 (2018).

[33] A. Ramos, K. Moore, and G. Raithel, Measuring the Rydberg constant using circular Rydberg atoms in an intensity-modulated optical lattice, Phys. Rev. A **96**, 032513 (2017).

[34] T. L. Nguyen, J. Raimond, C. Sayrin, R. Cortiñas, T. Cantat-Moltrecht, F. Assemat, I. Dotsenko, S. Gleyzes, S. Haroche, G. Roux, T. Jolicoeur, and M. Brune, Towards Quantum Simulation with Circular Rydberg Atoms, Phys. Rev. X **8**, 011032 (2018).

[35] F. Roussel, M. Cheret, L. Chen, T. Bolzinger, G. Spiess, J. Hare, and M. Gross, Observation of Circular-Metastable Doubly Excited States of Barium, Phys. Rev. Lett. **65**, 3112 (1990).

[36] F. Meinert, C. Hölzl, M. A. Nebioglu, A. D'Arnese, P. Karl, M. Dressel, and M. Scheffler, Indium tin oxide films meet circular Rydberg atoms: Prospects for novel quantum simulation schemes, Phys. Rev. Research **2**, 023192 (2020).

[37] See Supplemental Material at http://link.aps.org/supplemental/10.1103/PhysRevLett.125.263001 for additional details about the experimental set-up, the ionization signals, the singlet-triplet probes and the numerical model.

[38] B. A. Bushaw and W. Nortershauser, Resonance ionization spectroscopy of stable strontium isotopes and 90Sr via $5s21S0 \rightarrow 5s5p1P1 \rightarrow 5s5d1D2 \rightarrow 5s11f1F3 \rightarrow Sr^{+}$, At. Spectrosc. **55**, 1679 (2000).

[39] D. J. Berkeland and M. G. Boshier, Destabilization of dark states and optical spectroscopy in Zeeman-degenerate atomic systems, Phys. Rev. A **65**, 033413 (2002).

[40] H. Zhang, M. Gutierrez, G. H. Low, R. Rines, J. Stuart, T. Wu, and I. Chuang, Iterative precision measurement of branching ratios applied to 5 P states in $^{88}Sr^{+}$, New J. Phys. **18**, 123021 (2016).

[41] D. Leibfried, R. Blatt, C. Monroe, and D. Wineland, Quantum dynamics of single trapped ions, Rev. Mod. Phys. **75**, 281 (2003).